Investigation into Properties of Laser Welded Similar and Dissimilar Steel Joints

Article *in* Science and Technology of Welding & Joining · April 1998

DOI: 10.1179/stw.1998.3.4.177

Investigation into properties of laser welded similar and dissimilar steel joints

G. Çam, Ç. Yeni, S. Erim, V. Ventzke, and M. Koçak

Laser beam welding is currently used in the welding of steels, aluminium alloys, thin sheets, and dissimilar materials. This high power density welding process has unique advantages of cost effectiveness, deep penetration, narrow bead and heat affected zone (HAZ) widths, and low distortion compared to other conventional welding processes. However, the metallurgical and mechanical properties of laser welds and the response of conventional materials to this new process are not yet fully established. The welding process may lead to drastic changes in the microstructure with accompanying effects on the mechanical properties and, hence, on the performance of the joint. The thermal cycles associated with laser beam welding are generally much faster than those involved in the conventional arc welding processes. This leads to the formation of a rather small weld zone that exhibits locally a high hardness in the case of C–Mn structural steels owing to the formation of martensite. It is currently difficult to determine the tensile properties (full stress–strain curves) of the laser welded joint area owing to the small size (~2–3 mm) of the fusion zone. Complete information on the tensile and fracture toughness properties of the fusion zone is essential for prequalification and complete understanding of the joint performance in service, as well as for conducting a defect assessment procedure on such welded joints. Therefore, an experimental investigation into the mechanical properties of laser welded joints was carried out to establish a testing procedure using flat microtensile specimens (0·5 mm in thickness, 2 mm in width) for determination of the tensile properties of the weld metal and HAZ of the laser beam welds. Three similar joints, namely St 37–St 37, St 52–St 52, and austenitic–austenitic, and two dissimilar ferritic–austenitic joints were produced by CO_2 laser, using 6 mm thickness plates. The mechanical properties have been examined by microhardness survey and testing of conventional transverse tensile, round tensile, and flat microtensile specimens. The results for the microtensile specimens were compared with those for standard round tensile specimens and this clearly showed the suitability of the microtensile specimen technique for such joints.

Dr Çam, Dipl.-Phy. Ventzke, and Dr Koçak are at the GKSS Research Center, Institute of Materials Research, D-21502 Geesthacht, Germany and Dr Yeni and Dr Erim are in the Faculty of Engineering, Mechanical Engineering Department, Dokuz Eylül University, Izmir, Turkey. *Manuscript received 12 November 1997; in final form 16 December 1997.*

INTRODUCTION

The laser beam (LB) welding process has unique advantages of cost effectiveness, deep penetration, narrow bead width, and narrow heat affected zone (HAZ) development compared to conventional fusion welding processes.[1] Despite the high investment cost of laser welding equipment, it is expected that laser welding will have a great impact on fabrication and manufacturing industries for the welding of medium section steel structures within the next decade.[2] However, the significance of the metallurgical and mechanical properties of LB welds combined with the unique shape of the weld joint still needs to be established for structural components.

Laser welded joints, like all other weld joints, may contain defects in the form of cracks in the narrow weld area, or cracks may develop from inhomogeneities during service. The size and location of such cracks associated with characteristics of the local microstructure and the level of mechanical strength mismatch between the weld region and the parent plate under certain service conditions directly affect the joint performance and the lifetime of a structure. It is now known that the variation in mechanical properties of different regions (strength mismatch) of a conventional weld joint can significantly influence the deformation characteristics of welds in service. However, LB welding produces a very narrow weld bead and HAZ, which may be an advantage over conventional processes if the weld joint shows high hardness–strength (i.e. low toughness) owing to the occurrence of plastic deformation in the parent plate under external stresses. However, for prequalification or defect assessment purposes, the determination of the mechanical properties of a very narrow LB fusion zone can not be done by standard testing procedures. For instance, it is usually observed that transverse tensile specimens fail in the softer base metal and that fracture path deviation occurs in Charpy V notch and crack tip opening displacement (CTOD) fracture toughness testing of these welds owing to mechanical property mismatch between the base

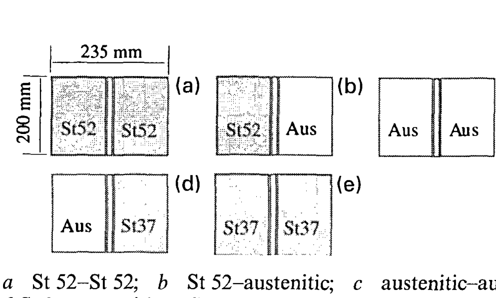

a St 52–St 52; *b* St 52–austenitic; *c* austenitic–austenitic; *d* St 37–austenitic; *e* St 37–St 37

1 Schematic illustration of LB welded joints: plate thickness 6 mm

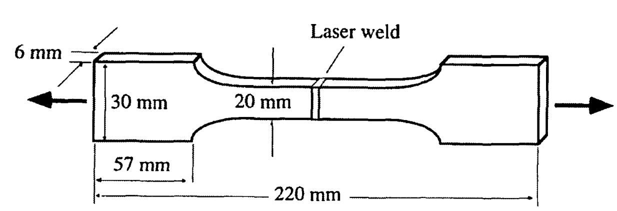

2 Standard transverse tensile specimen

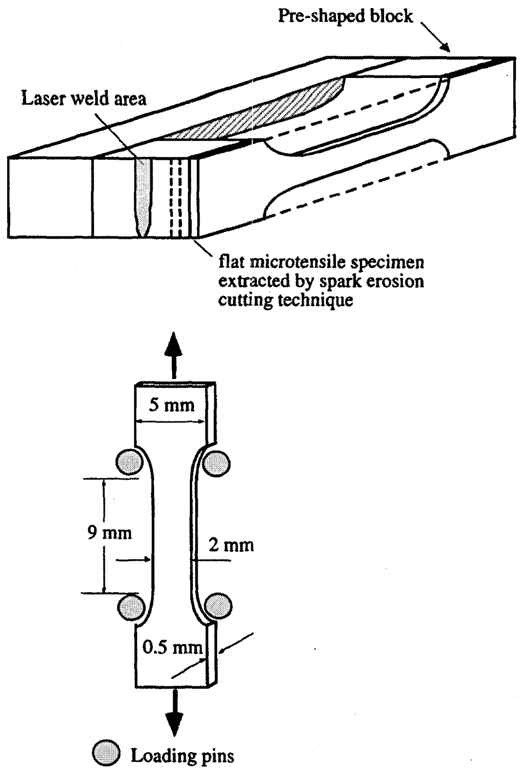

3 Extraction of microtensile specimens from LB welded plates

metal and the weld region. Therefore, these standardised test results may provide information only on the performance of the entire joint under tensile, impact, and bending loading conditions, respectively. They may fail in providing required intrinsic tensile and toughness properties of the fusion zone owing to interaction (unavoidable) between the weld region and the parent plate under applied deformation. For CTOD toughness determination, the effects of specimen geometry (weld width, crack size, notch position, etc.) and the degree of strength mismatch between the base metal and the weld region on toughness have to be taken into account.[3–11]

With regard to the establishment of the flat microtensile specimen testing procedure and, hence, determination of the tensile property gradient existing in the LB fusion zone, this particular work has been conducted. The flat microtensile specimen technique was originally developed for property determination in HAZs of conventional multipass weld joints used in the nuclear industry.[12] Successful applications of this technique to thick section similar and dissimilar electron beam welds[3] and to bond strength determination for diffusion bonded joints[13,14] have also been carried out at the GKSS Research Center. The present study is an extension of these experimental activities and specifically addresses the development and validation of the testing procedure for LB steel welds. Hence, similar and dissimilar LB weld joints between ferritic and austenitic steels produced by CO_2 laser using 6 mm thickness plates were systematically investigated.

EXPERIMENTAL

In the present study, austenitic stainless steel 1.4404 (X 2 Cr Ni Mo 18 10) and ferritic steels (grades St 37 and St 52) were used as the base metals. Similar and dissimilar single pass full penetration CO_2 LB welds were produced without using filler wire (Fig. 1). Extensive microhardness measurements (using 100 g load) were performed across the welded regions at three different locations, namely at the weld root, midsection, and top part of the joints. In addition, the narrow HAZ region of the ferritic steel was extensively screened by conducting microhardness measurements parallel to the fusion line.

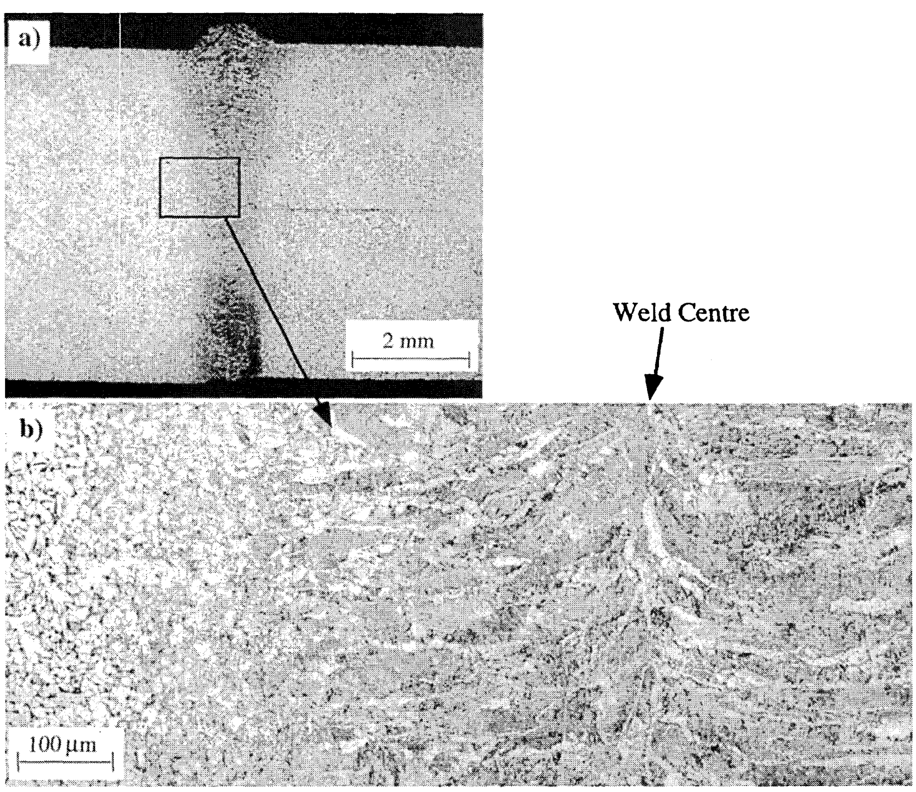

a macrosection; *b* higher magnification of region indicated in *a*

4 Similar St 37 LB joint

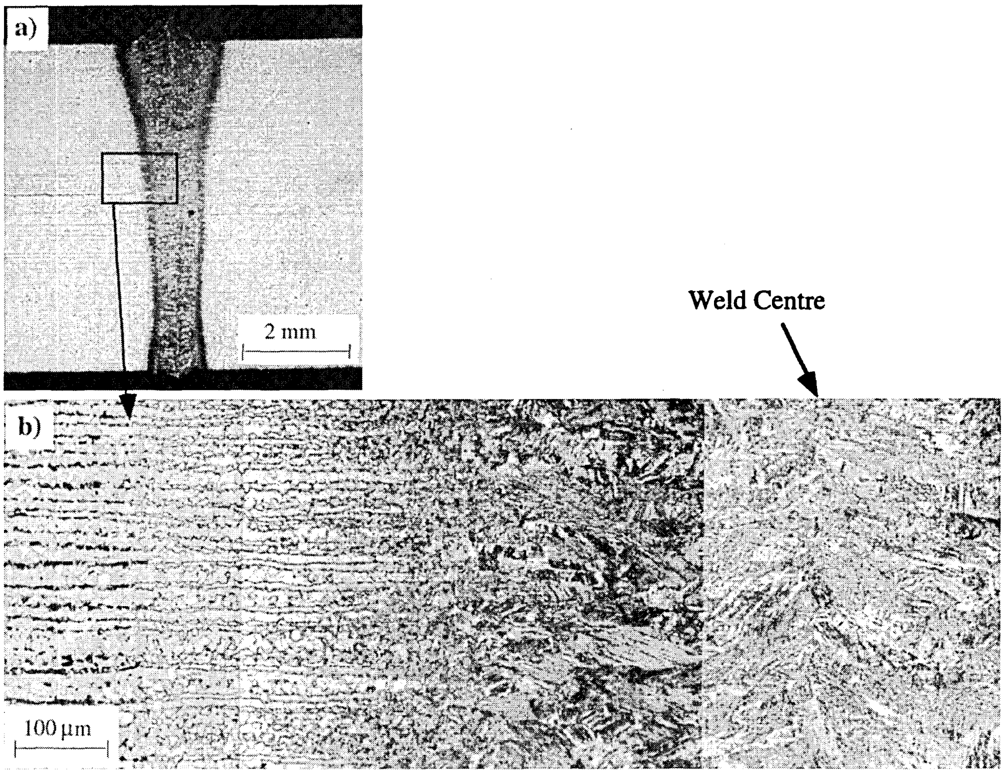

a macrosection; *b* higher magnification of region indicated in *a*

5 Similar St 52 LB joint

Standard flat transverse tensile specimens were extracted from the welded plates and tested at room temperature (Fig. 2). The weld reinforcement was machined before testing. Sets of flat microtensile specimens were extracted by spark erosion cutting from the base metals, HAZs, and weld metals of all the joints studied, as schematically shown in Fig. 3. The flat microtensile specimen preparation was conducted mainly in two stages: (a) extraction of a preshaped block with a laser weld in the centre; (b) cutting of specimens from the etched preshaped block using a spark erosion cutting technique (with 0·1 mm diameter copper wire) parallel to the weld. Owing to the small size of the microtensile specimens, loading was introduced using four high strength round pins at the shoulders of the specimens (Fig. 3). After testing, the broken half of each specimen was mounted for microstructural verification of the specimen location. The fracture surfaces of selected specimens were also examined by scanning electron microscopy.

For optical metallography, specimens were mounted in bakelite and ground with silicon carbide papers of 220, 400, 800, 1200, and 2400 grades followed by polishing on a rotating wheel with 7 and 2 µm diamond paste. Ferritic steels were etched with a solution comprising 2% nitric acid in alcohol for 10 s, while V_2A etchant, which consists of 100 mL distilled water, 100 mL HCl, 10 mL HNO_3, and 0·3 mL Vogels Sparbeize (etching solution), was used to etch austenitic steels at 70°C, the etching time being 5–10 s.

RESULTS AND DISCUSSION

Microstructural observations

Microstructural examination showed that the weld regions of all the joints with a ferritic constituent contained martensite and bainite. Ferritic–ferritic similar joints displayed a weld metal structure consisting of martensite and bainite (Figs. 4 and 5), whereas austenitic–austenitic similar welds exhibited an austenitic dendritic (cellular) structure with no evidence of martensite formation, as expected (Fig. 6). Solidification cracking was not observed in the austenitic similar weld, which might be a result of the very fine austenite cell size characteristic of the primary austenite solidification process of this steel grade. The HAZ in ferritic similar joints contained a refined ferrite–pearlite structure and pearlite dissolution at the base metal sides,

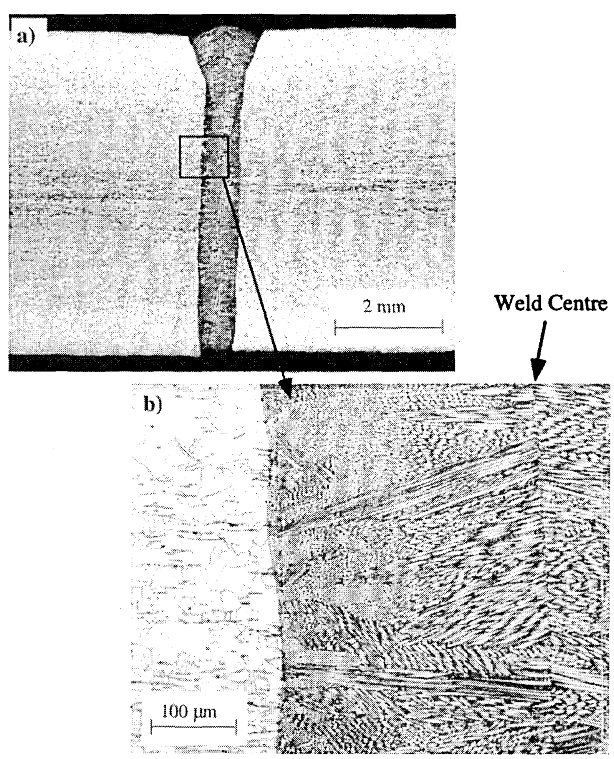

a macrosection; *b* higher magnification of region indicated in *a*

6 Similar austenitic LB joint

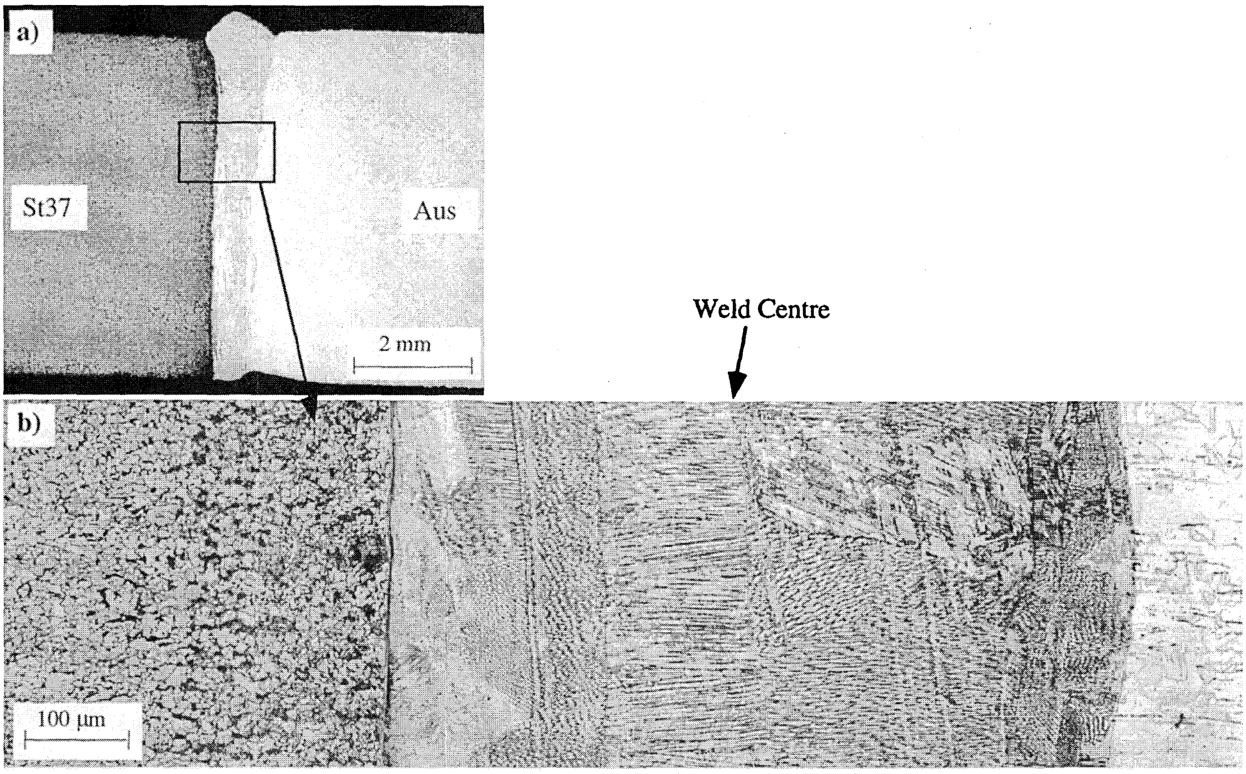

a macrosection; *b* higher magnification of region indicated in *a*

7 Dissimilar St 37–austenitic LB joint

while no distinct HAZ was observed in austenitic similar joints.

Ferritic–austenitic dissimilar joints, conversely, showed an inhomogeneous weld metal microstructure (Figs. 7 and 8). A narrow HAZ was observed on the ferritic steel side, in contrast to the austenitic side where there was no distinct HAZ.[15] This is typical of dissimilar steel LB weldments. The HAZ on the ferritic steel side of the St 37–austenitic joint contained no martensite, in contrast to that of the St 52–austenitic joint which exhibited some martensitic structure. The remainder of each weld in the centre displayed an inhomogeneous microstructure which contained

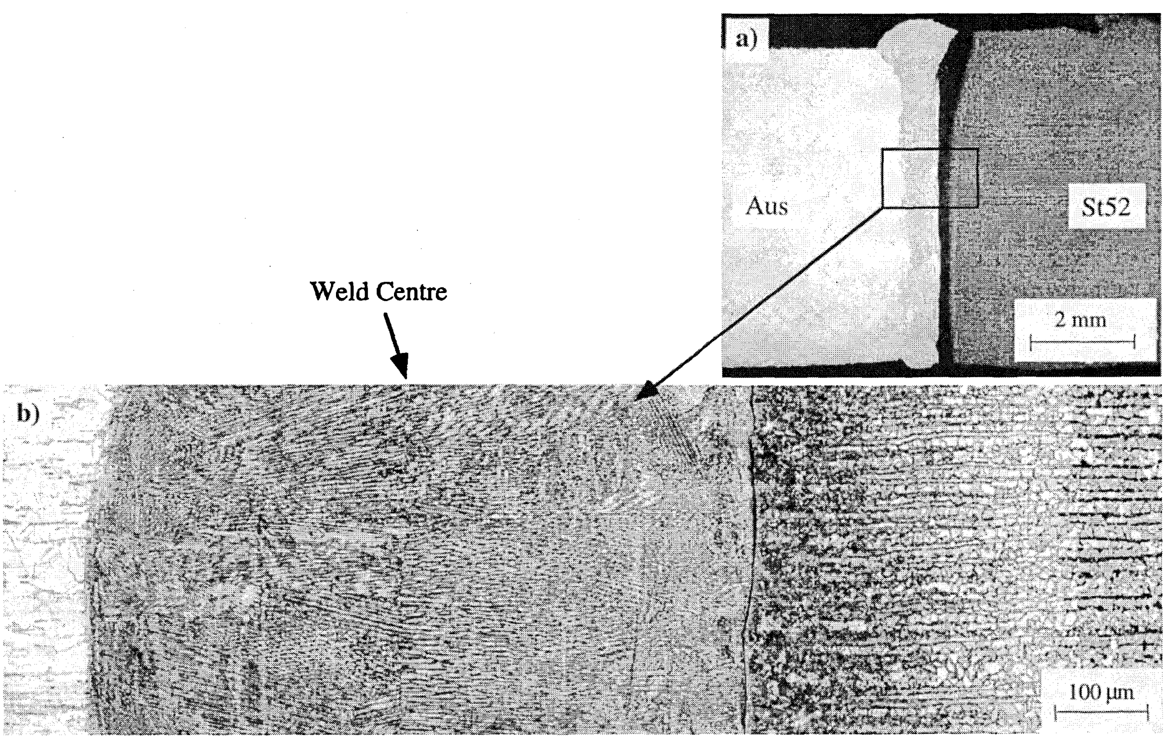

a macrosection; *b* higher magnification of region indicated in *a*

8 Dissimilar St 52–austenitic LB joint

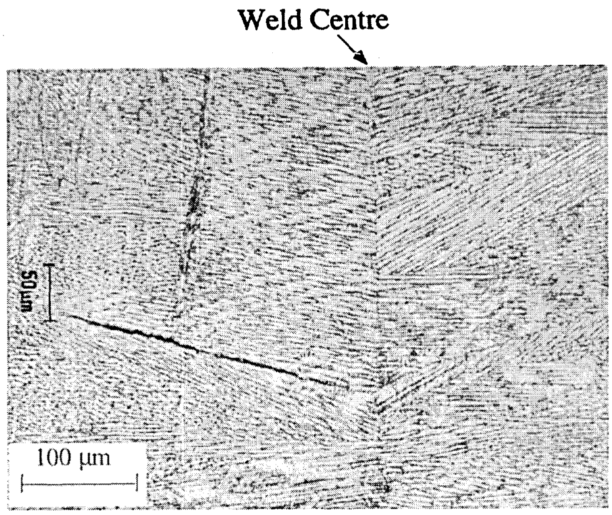

9 Solidification cracking in weld region of dissimilar joint

ferritic–austenitic and bainitic and/or martensitic phases in varying degrees, owing to an incomplete mixture of the molten metals of both sides in the weld pool during solidification. Some austenitic dendritic (cellular) structure was also observed at the austenitic steel side. Moreover, some solidification cracks were observed in the weld regions of the dissimilar joints (Fig. 9), which indicates that stress levels developed in these weldments sufficient to separate the grain boundaries in the cellular structure (presenting rather flat smooth crack paths) during solidification. It can also be assumed that low melting constituents were segregated along these boundaries, which resulted in solidification cracking during the final stages of solidification.

Microstructural examination and microhardness measurements were also carried out on the microtensile specimens to correlate the mechanical properties with the microstructure. Compositional analyses of the weld metals are currently in progress to correlate the microstructures with the Schaeffler diagram that was originally developed for conventional welds.

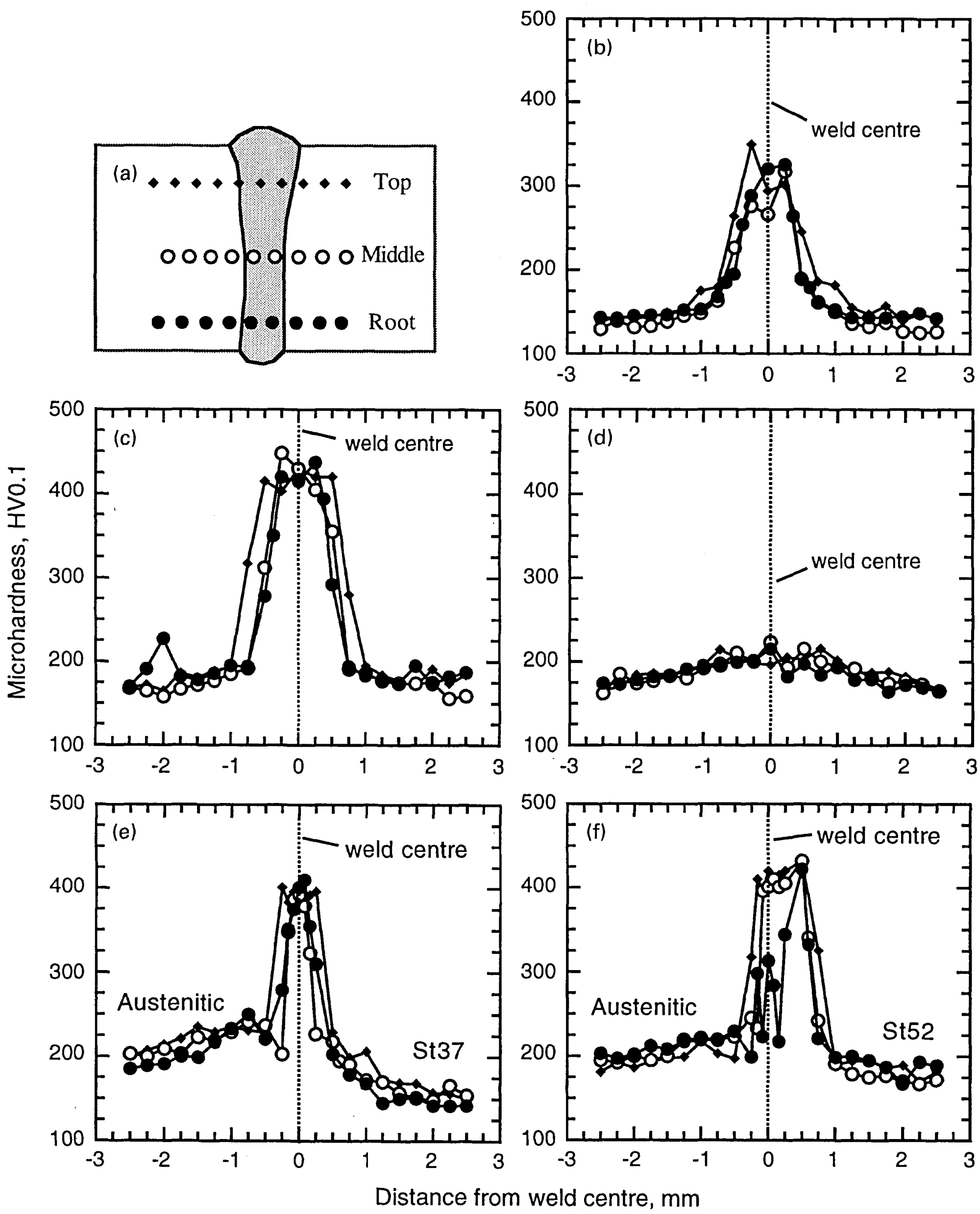

a schematic illustration of microhardness measurement procedure; *b* similar St 37; *c* similar St 52; *d* similar austenitic; *e* dissimilar St 37–austenitic; *f* dissimilar St 52–austenitic

10 Hardness profiles of joints

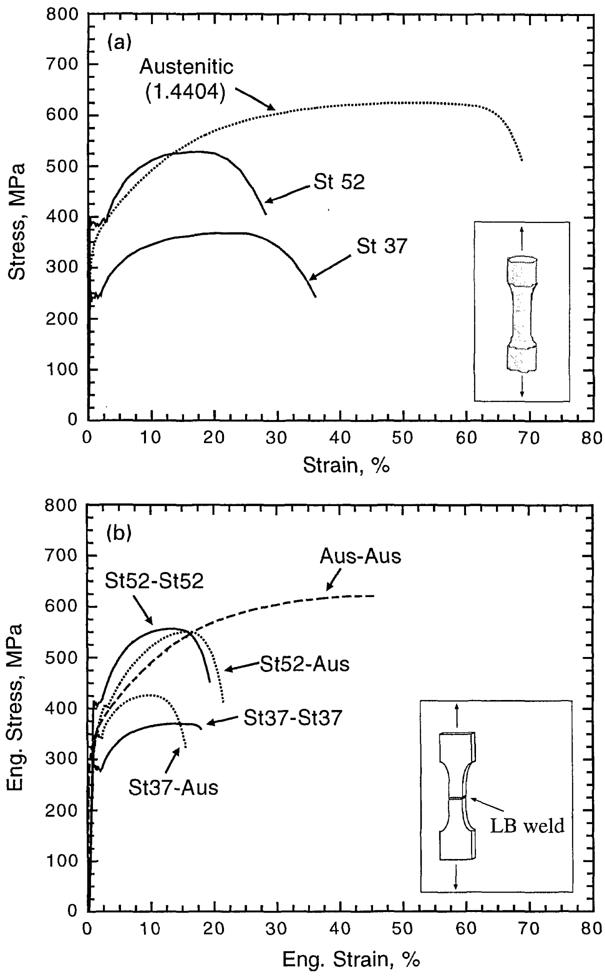

a base metals, standard round; *b* LB weld joints, transverse

11 Stress–strain curves for base metals and LB weld joints determined by testing given tensile specimens

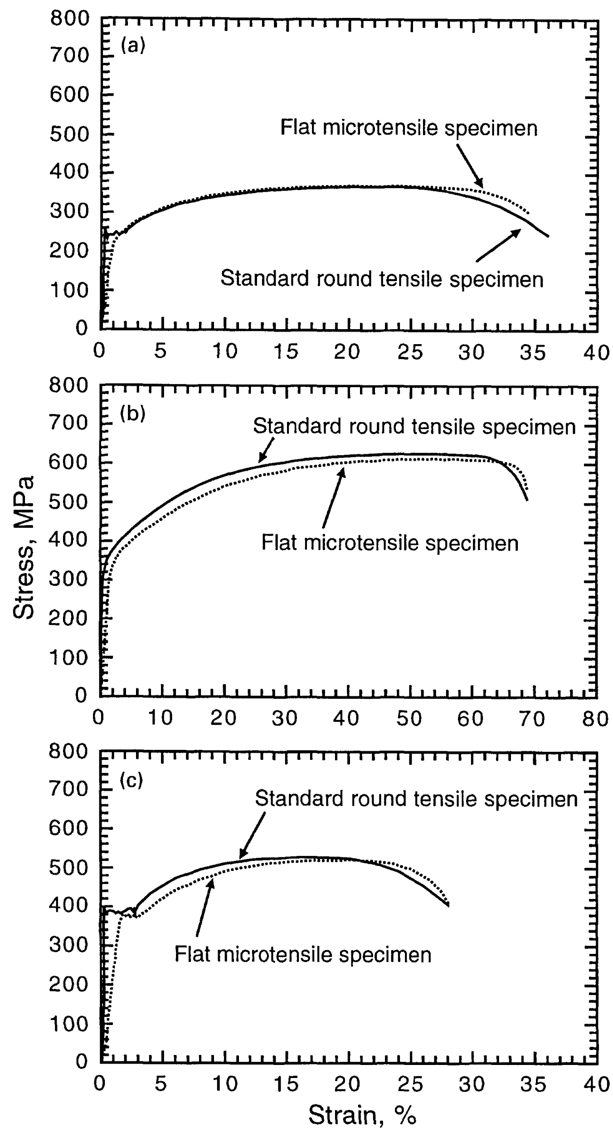

a St 37; *b* St 52; *c* austenitic steel

12 Comparison of stress–strain curves for base metals obtained by testing standard round and flat microtensile specimens

Hardness

The welding process may lead to drastic changes in the microstructure with accompanying effects on the properties of the joint. The thermal cycles associated with laser welding are generally faster than those involved in the conventional welding processes. This is a natural consequence of the low heat input and high welding speed (rapid cooling rate). It does mean, however, in C–Mn structural steels, that the weld region will exhibit locally high hardness values. To determine hardness profiles in the present work, extensive microhardness measurements were conducted at three locations (top, middle, and root) as shown in Fig. 10*a*. The microhardness results exhibited no significant difference between these three locations for all the welded joints studied. It can be concluded, therefore, that no significant gradient in mechanical properties of laser welds along the plate thickness direction is expected.

Similar ferritic steel joints displayed a high hardness profile in the weld region while similar austenitic welds showed no significant increase in hardness across the joint. Similar St 37 and St 52 joints exhibited hardness values of 270–350 HV0·1 (Fig. 10*b*) and 405–450 HV0·1 (Fig. 10*c*), respectively, whereas similar austenitic joints displayed hardness values of ~210 HV0·1 in the weld region (Fig. 10*d*). This is expected owing to the lack of bainite and/or martensite formation in the weld regions of austenitic joints. Dissimilar St 37–austenitic joints displayed a hardness peak in the weld metal which exhibited values of ~380–400 HV0·1. Dissimilar St 52–austenitic joints displayed a hardness peak of ~425 HV0·1 at the ferritic side, slightly higher than that of the weld metal which exhibited hardness values of ~400 HV0·1; this was caused by the presence of martensite in the narrow HAZ region at the ferritic side (designated as HAZ-F hereafter) as mentioned above. Higher hardness values obtained in the weld regions of ferritic similar and dissimilar joints resulted from the presence of bainite and/or martensite in the microstructure. Hardness profiles of the dissimilar joints are shown in Fig. 10*e* and *f*. The presence of high hardness peaks indicates the strength overmatching nature of the weld joints.

Mechanical properties

Standard round tensile specimens of the base metals were tested to determine the mismatch ratios *M* from the properties given in Table 1. Stress–strain curves for the round tensile specimens (diameter 4 mm, gauge length 20 mm) extracted from the base metals are shown in Fig. 11*a*. The yield strength mismatch ratios for the base plates of St 37–austenitic and St 52–austenitic dissimilar joints, $M = YS_{St\,37}/YS_{aus}$ and $M = YS_{aus}/YS_{St\,52}$, were found to be 0·76 and 0·8, respectively. Standard flat transverse tensile

Table 1 Mechanical properties of base metals*

Base metal	Yield strength, MPa	Tensile strength, MPa	Elongation, %	Reduction in area, %
St 37	233	368	36	51·06
St 52	382	528	30	50·58
Austenitic steel (1.4404)	308	626	69	49·61

* Mismatch ratios $M = YS_{St\,37}/YS_{aus}$ and $M = YS_{aus}/YS_{St\,52}$ where YS is yield strength.

specimens were also tested to determine the mechanical properties of the joints (Fig. 11*b*). Similar and dissimilar joints containing ferritic steel always failed in the lower strength ferritic base metal, owing to the very high hardness of the weld region. The stress–strain curves obtained for the flat transverse tensile specimens show some differences from those obtained for the round tensile specimens, owing to the presence of the LB weld region at the centre of the former specimens (Fig. 11). The stress–strain curves for the dissimilar joints lie between those of the similar joints of the constituent steels, as expected (Fig. 11*b*). Evidently, transverse tensile testing, particularly for ferritic steel containing joints where a very high hardness profile exists, does not give any information on the local mechanical properties of the weld region.

Stress–strain curves obtained for standard round and flat microtensile specimens of the base metals are compared in Fig. 12. Although there are slight differences between the curves owing to the different geometries of these two specimen types, they are in good agreement, which indicates that the flat microtensile specimen technique can be used to determine local mechanical properties of the narrow LB welds.

Hence, all weld metal and all HAZ flat microtensile specimens were prepared and tested to determine the local mechanical properties of the respective areas in the weld regions. Table 2 summarises the mechanical properties of the ferritic base metals (BM-F), austenitic base metal (BM-A), weld metals (WM), HAZs of the ferritic steels (HAZ-F), and HAZs of the austenitic steel (HAZ-A) in similar and dissimilar joints determined using microtensile specimens. The weld metal regions of the joints containing a ferritic constituent exhibited high strength (overmatching) and low strain values, whereas austenitic similar joints showed similar strength (even matching) and strain levels in the weld metal, HAZ, and base metal regions, as the microhardness results indicated. The strength mismatch ratios for the weld metal regions and the respective base metals (lower strength base material in the case of dissimilar joints), $M = YS_{WM}/YS_{BS}$, are also given in Table 2. The highest mismatch ($M = 3{\cdot}09$) existed between the weld metal and base metal of the similar St 37–St 37 joint. The full stress–strain curves for all specimens are shown in Fig. 13. The individual values of the yield strength (YS), tensile strength (TS), and fracture strain with respect to specimen location for all the joints are shown in Fig. 14. The characteristic microstructure for each microtensile specimen was checked (after testing) by optical metallography at the gauge length region of the specimens. Figures 15–19 show representative micrographs for all five weld joints. These results are discussed in detail below.

Ferritic similar joints

Figure 13*a* and *e* show the stress–strain curves for microtensile specimens extracted from the similar ferritic joints, and Fig. 14*a* and *e* show the variations in mechanical properties of these joints. As is seen from these figures, the weld metals, particularly in the case of St 52, exhibited the highest strength levels and the lowest strain values compared to the base metal and HAZ regions. The HAZ regions of these joints also exhibited higher strength levels and lower strain values than those of the respective base metals.

The microstructures of the weld metal, HAZ, and base metal specimens of the similar St 37 joint are shown in

Table 2 Summary of BM, HAZ, and WM mechanical properties* of LB welded joints† determined by testing of microtensile specimens: values in parentheses are averages

	St 37–St 37		St 37–austenitic		Austenitic–austenitic		St 52–austenitic		St 52–St 52	
	YS, MPa	TS, MPa	YS, MPa	TS, MPa	YS, MPa	TS, MPa	YS, MPa	TS, MPa	YS, MPa	TS, MPa
BM-F	230 (222)	370 (372)	330 (325)	419 (415)	...	...	355 (363)	545 (535)	369 (372)	523 (536)
	215	376	327	404	...	...	372	522	379	536
	215	367	334	440	...	...	371	529	384	541
	228	374	307	398	...	...	355	545	357	545
BM-A	...	...	326 (319)	593 (598)	316 (319)	611 (607)	312 (317)	607 (607)	...	...
	...	...	304	573	326	609	318	601	...	...
	...	...	320	608	318	601	318	617	...	...
	...	...	325	616	316	607	320	602	...	...
WM	640 (685)	825 (851)	900 (740)	988 (797)	360	552	745 (702)	998 (860)	980 (930)	1232 (1155)
	730	893	580	606	...	...	658	722	900	1141
	638	804	...	...	...	...	...	...	910	1092
	732	880	...	...	...	...	...	...	...	...
HAZ-F	320	432	416	496	...	...	580	757	620	870
	316	435	378	472	...	...	424	624	564	760
	298	421	718	823	...	...	...	...	382	557
	280	406	...	...	...	...	...	...	370	540
HAZ-A	...	...	424	591	448	621	438	668	...	...
	...	...	410	613	430	619	396	590	...	...
M‡	3·09		2·28		1·13		2·21		2·53	

* YS yield strength; TS tensile strength.
† F ferritic; A austenitic.
‡ $M = YS_{WM}/YS_{BM}$.

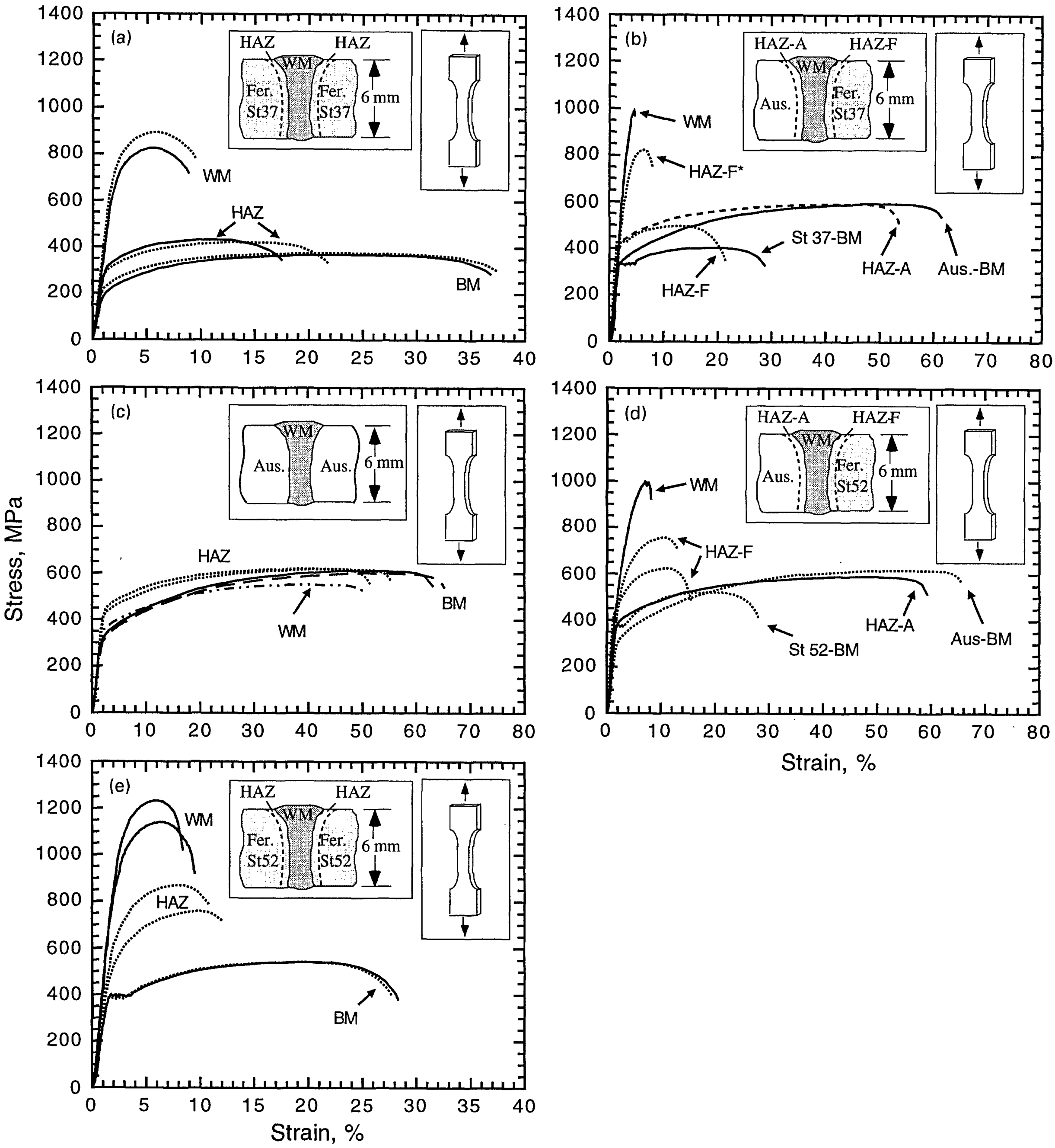

a similar St 37; *b* dissimilar St 37–austenitic (HAZ-F* next to fusion line); *c* similar austenitic; *d* dissimilar St 52–austenitic; *e* similar St 52

13 Stress–strain curves for flat microtensile specimens extracted from given joints

Fig. 15. The base metal microstructure consisted of coarse ferrite with some pearlite (Fig. 15*a*). The HAZ microtensile specimen displayed a similar microstructure of ferrite and pearlite containing finer regions (Fig. 15*b*), indicating that the specimen was extracted from the base metal side of the HAZ. The weld metal specimens, on the other hand, exhibited a microstructure comprising grain boundary ferrite with bainite and possibly martensite (Fig. 15*c*). The fracture surfaces of the all HAZ (extracted from the HAZ) and all WM (extracted from the weld metal) microtensile specimens of the similar St 37 joint exhibited a predominantly ductile failure mode (Fig. 20). The fracture surface of the all HAZ specimen displayed extensive dimple formation (Fig. 20*a*), whereas that of the all WM specimen exhibited the formation of a limited number of rather large voids and their coalescence (Fig. 20*b*).

The microstructures of the weld metal, HAZ, and base metal specimens of the similar St 52 joint are shown in Fig. 16. The base metal microstructure consisted of coarse ferrite with elongated pearlite (Fig. 16*a*). The HAZ microtensile specimen displayed a finer microstructure than that of the base metal, with pearlite dissolution (Fig. 16*b*). The weld metal specimen, on the other hand, exhibited a microstructure comprising martensite and bainite with some grain boundary ferrite (Fig. 16*c*). Fracture surfaces of the microtensile specimens extracted from this similar ferritic joint exhibited a predominantly ductile failure mode. Figure 21 shows the fracture surfaces of the all HAZ and all WM specimens. The fracture surface of the all HAZ specimen (Fig 21*a*) displayed a mixed brittle + ductile fracture mode (regions with a flat, brittle fracture appearance corresponding to the pearlite dissolution bands shown in

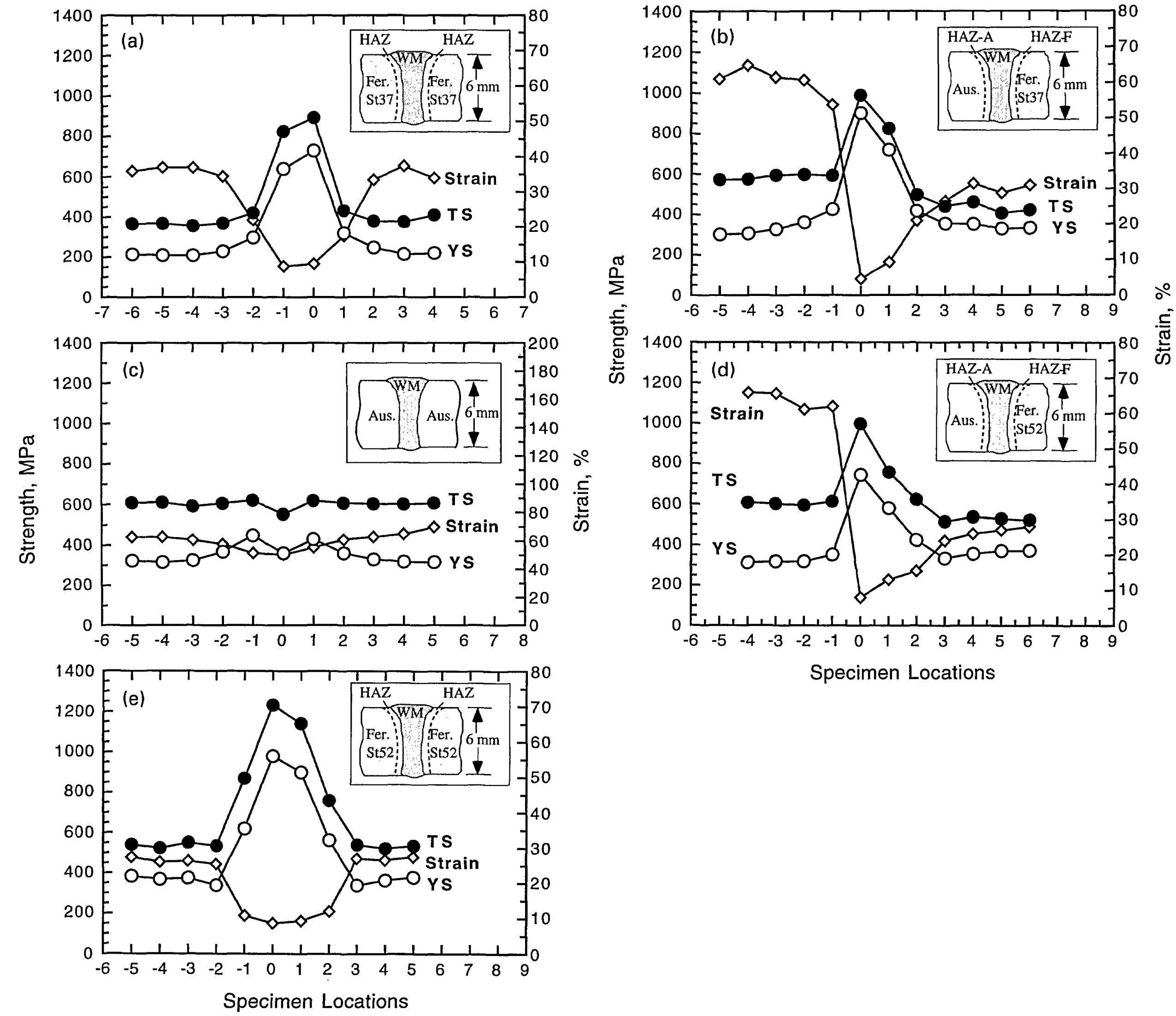

a similar St 37; *b* dissimilar St 37–austenitic; *c* similar austenitic; *d* dissimilar St 52–austenitic; *e* similar St 52

14 Mechanical property variations across joints: 0 represents weld centre

Fig. 16*b*), whereas that of the all WM specimen exhibited a predominantly brittle fracture mode (Fig. 21*b*).

Austenitic similar joint

For the austenitic similar joint, the weld metal and HAZ exhibited slightly lower strain values than that of the base metal with no significant alterations in the strength level (Figs. 13*c* and 14*c*). The microstructures of the base metal, HAZ, and weld metal specimens of the similar austenitic joint are shown in Fig. 17. The base metal and HAZ microtensile specimens exhibited similar microstructures consisting of austenite grains with some δ ferrite, indicating that there is no appreciable alteration in the microstructure in the HAZ of austenitic steel joints (Fig. 17*a* and *b*). The weld metal specimen displayed a homogeneous dendritic structure (Fig. 17*c*). Fracture surfaces of the microtensile specimens extracted from the similar austenitic joint also exhibited a predominantly ductile failure mode. Figure 22 shows the fracture surfaces of the all HAZ and all WM specimens. The fracture surface of the all HAZ specimen displayed extensive dimple formation (Fig. 22*a*), whereas that of the all WM specimen exhibited the formation of limited and coarse voids and their coalescence (Fig. 22*b*).

Dissimilar joints
(St 37–austenitic and St 52–austenitic)

In dissimilar joints, the weld metals exhibited the highest strength levels with limited strain values as seen in Figs. 13*b* and *d* and 14*b* and *d*. The reason for the extremely low strain values exhibited by the weld metals is the presence of harder microstructural constituents (bainite/martensite) as well as the solidification cracks in these regions as seen in Fig. 9. The HAZs at the ferritic sides (HAZ-F) also displayed relatively higher strength levels and lower strain values than those of the respective ferritic base metals. The HAZs at the austenitic sides (HAZ-A), on the other hand, did not exhibit a significant increase in strength, but some decrease in strain value compared to the austenitic base metal.

The microstructures of the weld metal, HAZ, and base metal specimens of the dissimilar St 37–austenitic joint are shown in Fig. 18. The ferritic base metal specimen exhibited a microstructure comprising ferrite and some pearlite (Fig. 18*a*). However, the microstructure was significantly finer than that of the base metal of the ferritic similar joint, which is the reason for the different stress–strain curves obtained (Fig. 13*a* and *b*). The difference between the strengths of the St 37 base metals of similar and dissimilar joints is indicated in Table 2. This difference is a result of

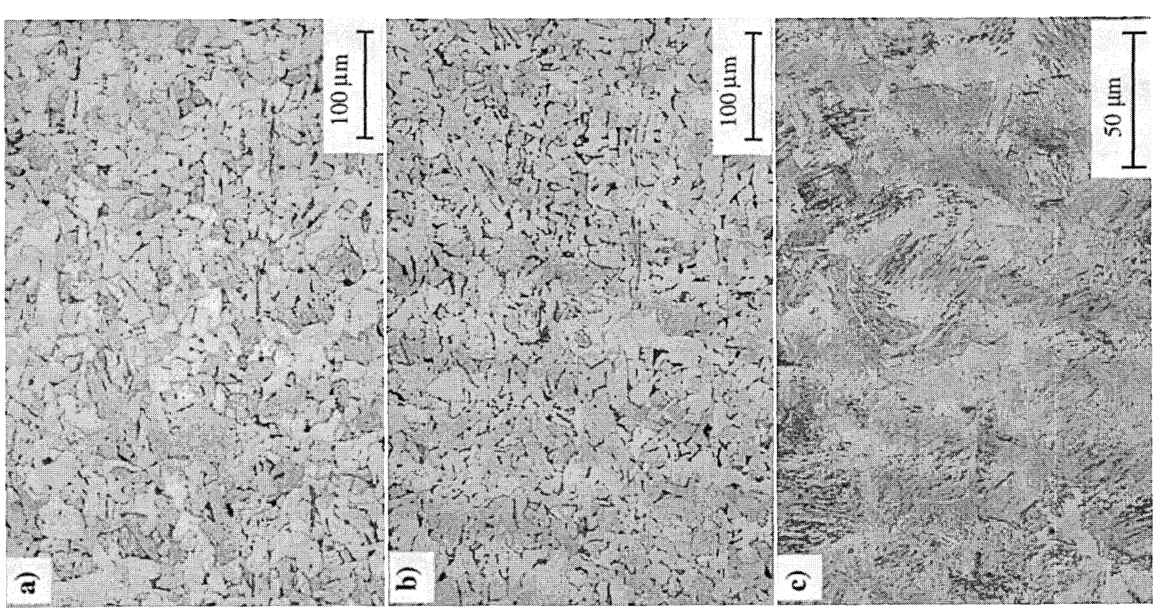

a base metal; *b* HAZ; *c* weld metal

15 Optical micrographs of microtensile specimens of similar St 37 joint extracted from given locations

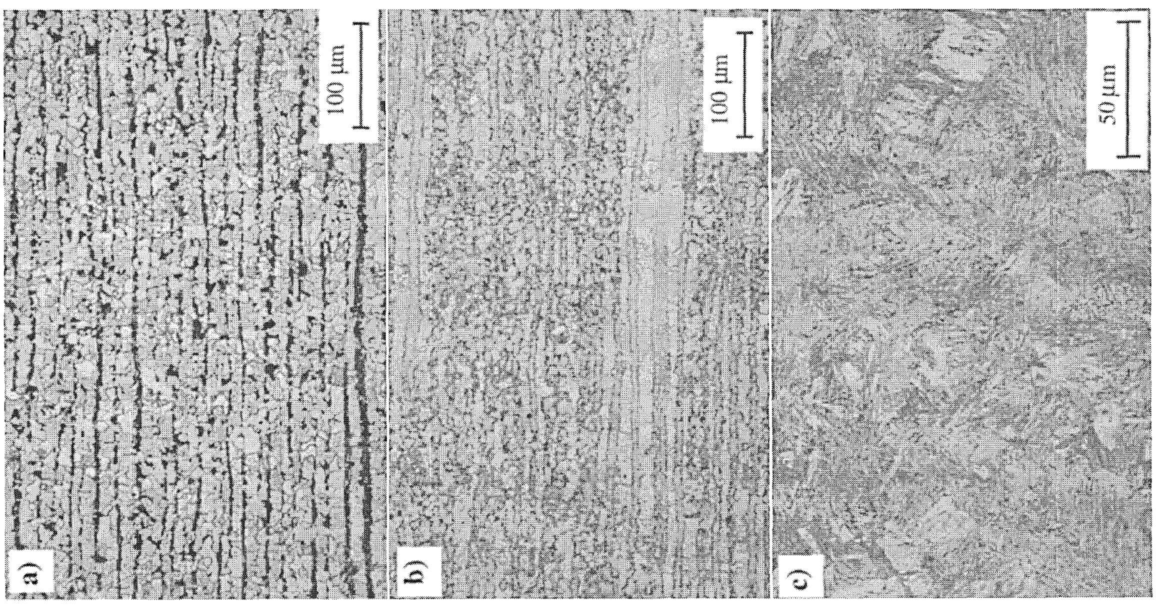

a base metal; *b* HAZ; *c* weld metal

16 Optical micrographs of microtensile specimens of similar St 52 joint extracted from given locations

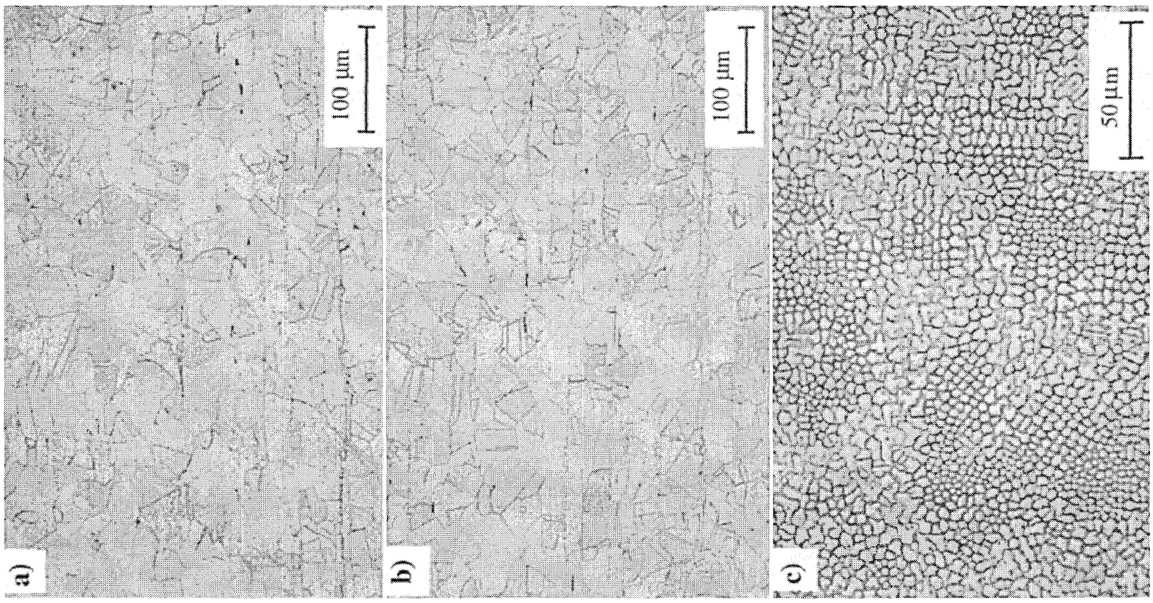

a base metal; *b* HAZ; *c* weld metal

17 Optical micrographs of microtensile specimens of similar austenitic joint extracted from given locations

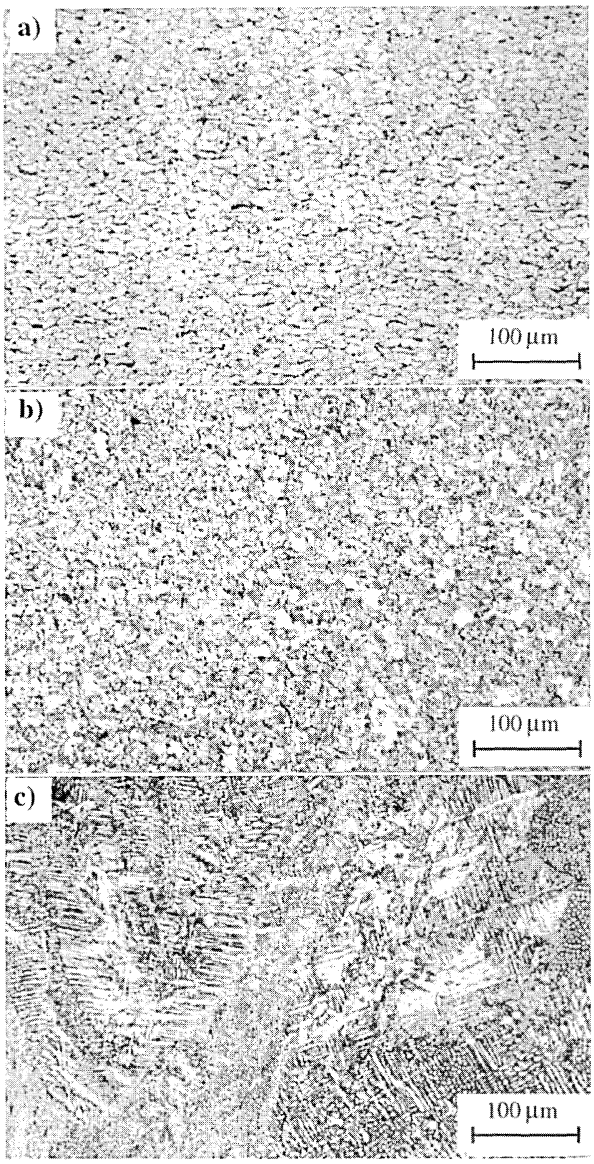

a ferritic base metal; *b* HAZ-F; *c* weld metal

18 Optical micrographs of microtensile specimens of dissimilar St 37–austenitic joint extracted from given locations

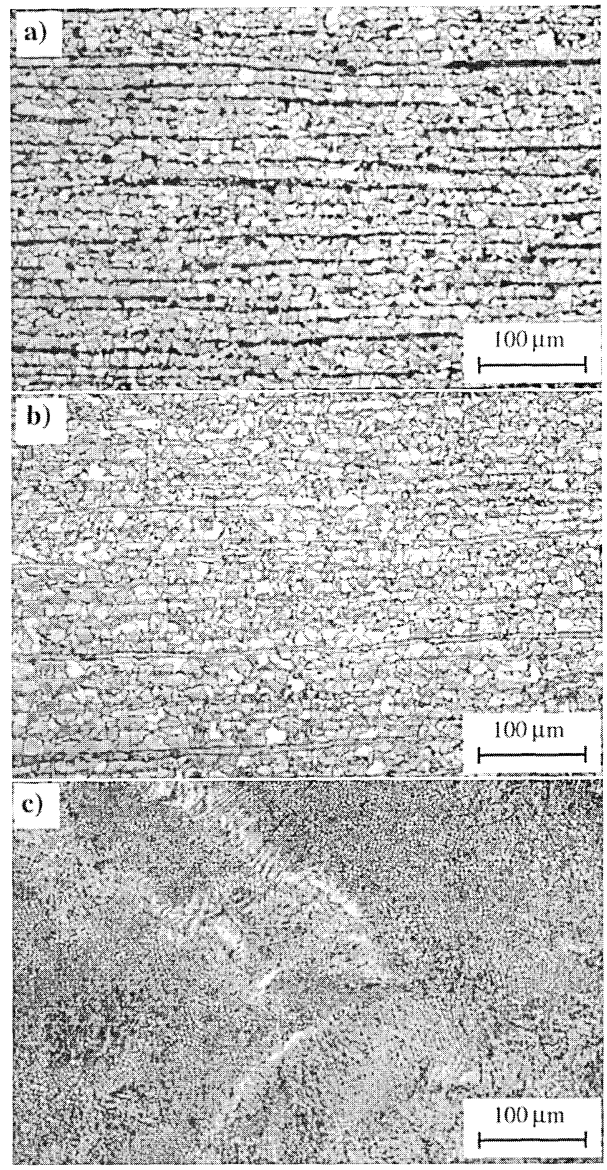

a ferritic base metal; *b* HAZ-F; *c* weld metal

19 Optical micrographs of microtensile specimens of dissimilar St 52–austenitic joint extracted from given locations

the different welding directions with respect to the rolling directions in similar and dissimilar joints of the St 37 grade. The HAZ at the ferritic side (HAZ-F) exhibited a much finer ferrite + pearlite structure than that of the ferritic base metal (Fig. 18*b*). The weld metal specimen, on the other hand, displayed an inhomogeneous microstructure containing a mixture of ferrite and austenite solidification structures (Fig. 18*c*). The HAZ at the austenite side (HAZ-A) and the austenitic base metal displayed a microstructure similar to that shown in Fig. 17*a* and *b*.

The microstructures of the weld metal HAZ, and base metal specimens of the dissimilar St 52–austenitic joint are shown in Fig. 19. The ferritic base metal specimen exhibited a microstructure comprising ferrite with elongated pearlite (Fig. 19*a*). The HAZ at the ferritic side (HAZ-F) exhibited a finer microstructure than that of the ferritic base metal with pearlite dissolution (Fig. 19*b*). Although a very narrow region of martensite had been previously observed in the HAZ-F in this joint, as also indicated by the hardness transverse, the microtensile specimen microstructure did not reveal this phase as this small region was not sampled in the extraction of the specimens. The weld metal specimen, on the other hand, displayed an inhomogeneous microstructure containing a mixture of ferrite and austenite solidification structures (Fig. 19*c*). The HAZ at the austenitic side (HAZ-A) and the austenitic base metal displayed a microstructure similar to that shown in Fig. 17*a* and *b*.

Fracture surfaces of the microtensile specimens extracted from the base metals and the HAZs of the dissimilar joints also exhibited a predominantly ductile failure mode. However, the all WM specimens exhibited a non-uniform fracture surface, which consisted of ductile regions and cleavage fracture of the dendritic zones (Fig. 23). Figure 23*a* shows the fracture surface of the dendritic region where some microplastic zones were clearly seen. Figure 23*b* illustrates a correspondence with the optical micrograph of the dendritic structure formed in the weld region (Fig. 9).

As discussed above, the mechanical properties (including full stress–strain curves) of each zone of LB welded similar and dissimilar joints can be successfully determined using the flat microtensile specimen technique. Complete information (not only hardness values) relating to the local mechanical properties of laser welds is often essential for

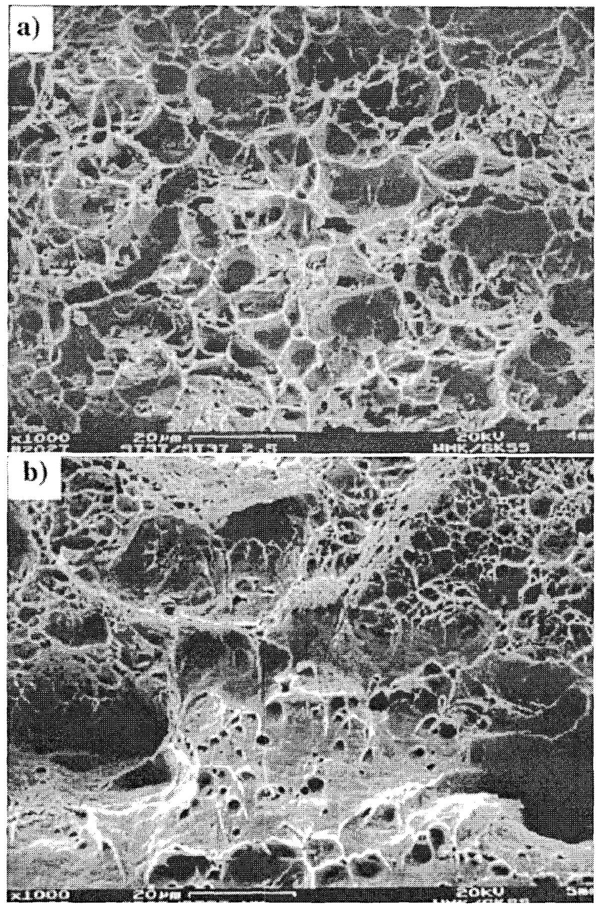

a fracture surface of HAZ showing extensive void formation; *b* fracture surface of WM showing limited void formation

20 Fracture surfaces of HAZ and WM of similar St 37 joint

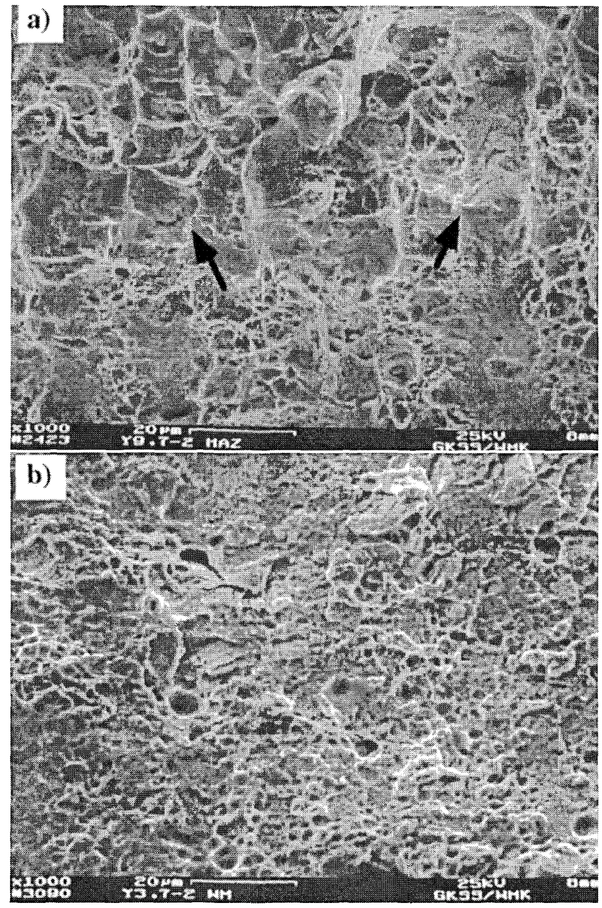

a fracture surface of HAZ showing mixed brittle + ductile mode of fracture (regions with flat, brittle fracture appearance indicated by arrows corresponding to pearlite dissolution bands shown in Fig. 16*b*); *b* fracture surface of WM showing predominantly brittle fracture mode

21 Fracture surfaces of HAZ and WM of similar St 52 joint

optimisation of the laser welding process and filler wire development for various alloys, as well as quality control and fracture mechanics analyses (experimental and numerical) of the welds. Development of filler wire compositions to reduce the level of hardenability of C–Mn steel joints and the level of softening of aluminium alloy weld joints is currently of great interest. To take a step forward in these areas, complete information regarding the local properties of actual weld joints should be generated. The testing technique described in the present paper can provide such information.

The present results are part of a large project carried out at the GKSS Research Center on the microstructural and mechanical characterisation of LB welded steels. The correlation of microhardness measurements conducted on microtensile specimens with mechanical properties of the respective areas of the joints is currently being conducted. Fracture toughness (CTOD) testing of the joints at room and low temperatures is also currently in progress and the results will be reported in a future publication.

CONCLUSIONS

1. The microstructures of CO_2 laser welded C–Mn steels contain large proportions of bainite/martensite in the weld region owing to the rapid cooling involved. Thus, an extreme hardness increase in the weld regions of ferritic similar and ferritic–austenitic dissimilar joints was observed in contrast to similar austenitic joints, the weld region of which displayed no significant hardness alteration.

2. All transverse tensile specimens failed at the lower strength base metal sides owing to the strength mismatch effect. Even the presence of some solidification cracks in dissimilar joints did not change the fracture location caused by the strength overmatching of the weld region.

3. Microtensile specimens extracted from the weld metals of similar ferritic joints displayed significantly higher strength values and markedly lower strain values than those of specimens extracted from the respective base metals, owing to the presence of bainite/martensite in the weld regions. The all HAZ specimens also exhibited higher strength values and lower strain values than those of the base metals. The base metal, HAZ, and weld metal of similar austenitic steel joints exhibited similar strength and strain values, as expected, since no hardness peak was observed in these joints.

4. Microtensile specimens extracted from the weld zones of dissimilar joints exhibited high strength and low strain values. The all HAZ specimens extracted from the HAZs at the ferritic sides also displayed higher strength and lower strain values than those of the respective ferritic base metals, whereas the specimens extracted from the HAZs at the austenitic sides and the austenitic base metals away from the weld regions exhibited similar strength and strain values with no significant alteration.

5. Finally, successful application of the flat microtensile specimen technique to laser welded joints, which exhibit very narrow weld regions, was demonstrated. By using this technique it is possible to determine the local mechanical properties of joints which can be correlated with the respective microstructure and hardness.

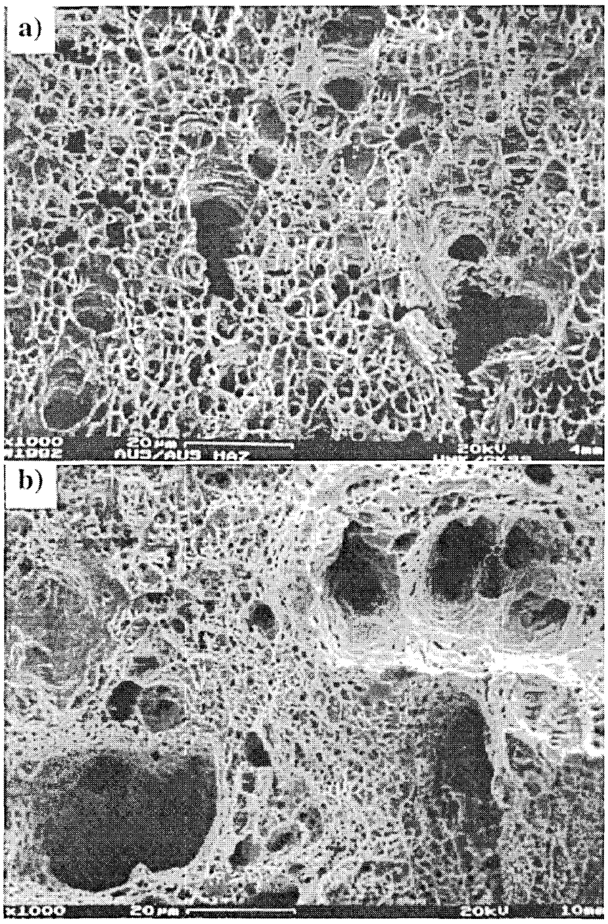

a fracture surface of HAZ showing extensive void formation; *b* fracture surface of WM showing limited void formation

22 Fracture surfaces of HAZ and WM of similar austenitic joint

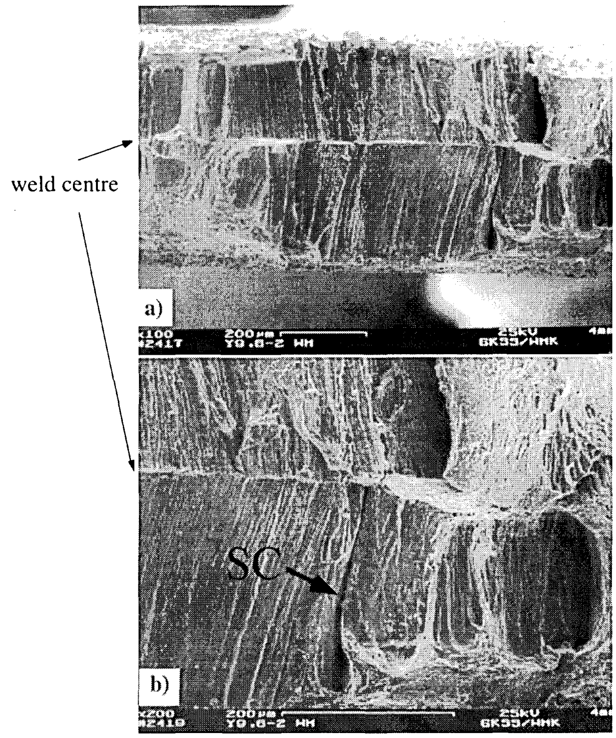

a overview showing complete thickness of microtensile specimen; *b* higher magnification of *a* showing existing solidification cracking (SC) in weld metal (also shown in Fig. 9)

23 Fracture surface WM of dissimilar joint

ACKNOWLEDGEMENTS

This work is part of the German–Turkish joint project financed by International Bureau, KFA-Jülich and Türkiye Bilimsel Teknik Arastirma Kurumu, Turkey. The authors would like to thank both organisations for their financial support. They would also like to thank H. Mackel and S. Riekehr for their technical assistance in testing. The metallography work of W.-V. Schmitz and P.-M. Fischer is also greatly appreciated.

REFERENCES

1. J. MAZUMDER: 'ASM handbook', Vol. 6, 'Welding, brazing and soldering', 262–269; 1993, Materials Park, OH, ASM International.
2. E. A. METZBOWER: Proc. 'Indo-US workshops on solidification principles and materials processing', Hyderabad, India, January 1988, Vol. 22–25, 655–669.
3. M. KOÇAK and E. JUNGHANS: Proc. 2nd European Conf. on Joining Technology, Florence, Italy, May 1994, Italian Institute of Welding.
4. J. K. KRISTENSEN: Proc. Conf. 'Exploitation of laser processing in shipyards and structural steelworks', Glasgow, UK, May 1996.
5. M. KOÇAK and K.-H. SCHWALBE: 'Neu Entwicklungen im konstruktiven Ingenieurbau', (ed. H. Saal and Ö. Bucak), 137–155; 1994, Karlsruhe, University of Karlsruhe.
6. J. K. KRISTENSEN and K. BORGREEN: Proc. 5th European Conf. on Laser Treatment of Materials, Bremen-Vegesack, Germany, September 1994, Bremer Institut für Angewandte Strahltechnik.
7. K.-H. SCHWALBE and M. KOÇAK: Proc. 3rd Int. Conf. on Trends in Welding Research, Gatlinburg, TN, USA, June 1992, ASM International, (ed. S. A. David and J. M. Vitek), 479–494; 1992, Materials Park, OH, ASM International.
8. Z. SUN and T. MOISIO: *Weld. J.*, April 1994, 63–70.
9. M. KOÇAK, M. ES-SOUNI, L. CHEN, and K.-H. SCHWALBE: Proc. 8th Int. Conf. and Exhibition on Offshore Mechanics and Arctic Engineering, The Hague, The Netherlands, March 1989, ASME, 623–633.
10. M. T. KIRK and R. H. DOODS: Report, UILU-ENG-92-2005, University of Illinois, Urbana, IL, 1992.
11. H. C. CAO and A. G. EVANS: *Mech. Mater.*, 1989, **7**, 295–304.
12. E. KLAUSNITZER: *Materialprüfung*, 1976, **11**, 411–416.
13. G. ÇAM, K.-H. BOHM, J. MÜLLAUER, and M. KOÇAK: *JOM*, 1996, **48**, (11), 66–68.
14. G. ÇAM, J. MÜLLAUER, and M. KOÇAK: *Sci. Technol. Weld. Joining*, 1997, **2**, (5), 213–219.
15. Ç. YENI, S. ERIM, G. ÇAM, and M. KOÇAK: Proc. Int. Symp. Welding Technology '96, Istanbul, Turkey, May 1996, Gedik Education Foundation, 235–247.